minerals

MDPI

Article

Dissolution of Carbonate Rocks in a Laboratory Setting: Rates and Textures

Erik B. Larson [1,*] and Ronald V. Emmons [1,2]

[1] Department of Natural Sciences, Shawnee State University, 940 Second St, Portsmouth, OH 45662, USA; Ronald.Emmons@rockets.utoledo.edu
[2] Department of Chemistry and Biochemistry, The University of Toledo, 2801 W. Bancroft St, Toledo, OH 43606, USA
* Correspondence: elarson@shawnee.edu; Tel.: +1-740-351-3144

Abstract: Determining the dissolution rates of carbonate rocks is vital to advancing our understanding of cave, karst, and landscape processes. Furthermore, the role of carbonate dissolution is important for the global carbon budget and climate change. A laboratory experiment was setup to calculate the dissolution rates of two whole rock carbonate samples with different petrographic makeup (ooids and brachiopods). The carbonate rock samples were also explored under a scanning electron microscope to evaluate the textures that developed after dissolution The oolitic limestone dissolved at a rate of 1579 cm yr^{-1}, and the pentamerous limestone (dolostone) dissolved at a rate of 799 cm yr^{-1}. Both rocks did not dissolve evenly across their surface as indicated by scanning electron microscopy, it appears the allochems dissolved preferentially to the matrix/cement of the rocks and that some mechanical weathering happened as well. This work reports that the petrography and mineralogy of carbonate rocks is important to consider when exploring the cave, karst, and landscape evolution and that attention should be paid to the petrography of carbonate rocks when considering the global carbon budget.

Keywords: carbonate rock; dissolution; denudation; karst; global carbon budget; climate change; micro-textures; laboratory experiment; atomic emission spectroscopy; scanning electron microscope

Citation: Larson, E.B.; Emmons, R.V. Dissolution of Carbonate Rocks in a Laboratory Setting: Rates and Textures. *Minerals* **2021**, *11*, 605. https://doi.org/10.3390/min11060605

Academic Editors: Barbara Woronko and Maciej Dąbski

Received: 28 April 2021
Accepted: 2 June 2021
Published: 5 June 2021

1. Introduction

Calculating the dissolution rate of carbonate rocks is vital for understanding cave, karst, and landscape processes. Recently there has also been a push to understand the role that karst processes may have on the global carbon budget in light of the continued climate change (e.g., [1,2]). Numerous approaches to calculating the dissolution rates of carbonate rocks have been applied over the past century which can be broadly placed into three categories: theory-based methods, field-based methods, and laboratory-based methods (e.g., [3–5])—explored in detail in the background section of the paper. To this point there has been relatively little attention paid to the petrology and petrography of these carbonate rocks as whole rocks (i.e., not powdered) in karstic studies. This study proposes a laboratory-based approach to quantifying carbonate rock (limestone and dolostone) dissolution rates through karstic processes while at the same time exploring the differential dissolution that happens to these whole carbonate rocks through karstic processes.

The approach described in this paper accounts for petrographic differences in carbonate rocks using powder x-ray powder diffraction (XRD) to determine their mineralogy and petrographic thin sections to describe the petrography of the rock. The dissolution rate of the carbonate rocks is determined using atomic emission spectroscopy (AES) of the water the rocks were dissolved in with CO_2. Scanning electron microscopy (SEM) was further used to describe the micro-scale textures developed on the rock during dissolution and identify uneven dissolution of the allochems in the rocks which has been poorly explored. To this point there have not been any studies that have investigated the dissolution of

whole carbonate rocks, their petrography, and their uneven dissolutional micro-textures. Hence, this paper attempts to address the nature of the karst environment on carbonate rocks holistically in a laboratory setting.

2. Background Information

Approaches to understanding the dissolution rates of carbonate rocks through attempts at first principles and modeling have advanced significantly over the last 60 years. Early attempts were made by Corbel [6] to calculate the denudation rates based on runoff in a watershed and determined that climate was the controlling factor of karstic denudation. While there were ultimately many issues with Corbel's [6] attempts, it stimulated an interest in calculating dissolution rates and formed the basis for much of what is considered today in calculating carbonate rock dissolution rates [7,8].

While there are many nuances (explored below) to the methods used for measuring carbonate rock dissolution rates, this paper will broadly focus on three large sub-fields: theory, field methods, and laboratory methods. Ford and Williams [3], Gabrovšek [4], and White [5] provide an excellent introductory overview to many of these methods.

2.1. Theory-Based Methods for Dissolution

The kinetics of carbonate rock dissolution has been actively investigated since the 1960s and can be explored in detail in the reviews from Dreybrodt [9], Ford and Williams [3], Morse and Arvidson [10], Morse et al. [11], and White [5] and references therein of all of them. Of significant importance to larger scale karst processes and carbonate dissolution is White's [12] model for theoretical maximal dissolution. This model [12] allowed for the accounting of precipitation, evaporation, temperature, CO_2 concentration, and the density of the rock in determining the maximum possible dissolution rate of carbonate rocks. White's [12] equation is used as the standard for calculating maximum theoretical dissolution rates [3,4].

2.2. Field-Based Methods for Dissolution

The major field-based methods for measuring the dissolution rates of carbonate rocks typically depend on: (1) Using limestone tables and measuring chances in mass (e.g., [13,14]); (2) using some sort of karrentisch/pedestals/differential weathering to physically measure landscape lowering (e.g., [4,15]); (3) hydrochemical analysis of watersheds to measure the makeup of discharging waters (e.g., [3–5]); or (4) microerosion meters to physically measure landscape lowering (e.g., [15,16]).

One of the most commonly used methods for observing the changes in mass of a sample is that proposed by Trudgill [13], which involved making a polished disc of rock which is placed in a dissolutional environment and then removed at some future date and weighed again to determine the amount of material dissolved (e.g., [3,4,14,15,17]). This method of measuring dissolution from a table has been applied extensively in cave settings, streams, and in soils (e.g., [3,4,14,15]). This method excels in that it places the rock sample in a more authentic dissolutional environment than the lab setting, albeit one at least somewhat altered to get the sample emplaced there [4,14,15]. The longer a sample is in place the more representative the dissolution rate becomes as climatic conditions begin to average out over time [4,14,15,17]. This method's weaknesses are the time it takes to process a sample, ensuring uniform sample characteristics (e.g., density, size, smoothness), and ensuring even/equal treatment of the samples through the entire process [4,14,15,17]

The use of karrentisch/pedestals/differential weathering to measure limestone dissolution is simple as it only requires a direct measurement of the surface relative to a benchmark feature, be that a resistant mineral (e.g., quartz vein), a cap rock, or an anthropogenic feature [3,4,15, and references therein]. These methods can be used over short time scales (decades–centuries) if using anthropogenic features as the benchmark, or millennia if relative to a different rock/lithology or in regions where other direct methods would be difficult [4,15]. The use of different rocks as the benchmark may be problematic as all rocks

weather to some degree and the timing of exposure may also be difficult to ascertain [4,15]. The use of anthropogenic material suffers from the possibility that the benchmark feature and the limestone may not have exposed and started dissolving flush to each other [4,15].

The hydrogeochemical analysis of water leaving a watershed can provide information about the amount of carbonate material dissolved in the watershed [3–5]. Corbel [6] first attempted to quantify this based on climatic variables, however he made too many simplifications in his model for it to really represent the reality of landscape scale karstic dissolution [7,8]. The modern advancement of this method excels in that continuous monitoring in the watershed can paint a full picture of changes of dissolution over time, however the method does not resolve the issues related to auto- and allogenic runoff nor do they account for any water that may enter the subsurface [3–5, and references therein].

The measurement of rock denudation by use of a microerosion meter allows for discrete measurements of landscape lowering over time [3,4,15]. These methods generally involve the placement of studs into the rock so that the microerosion meter can be placed at the same exact location over the length of the experiment—the probe then records the distance to the land surface from its stud benchmark to record the amount of landscape lowering that has happened [4,15]. This method provides high resolution, short-term denudation rates, however it is problematic when used on dissected surfaces, softer rocks which may be susceptible to mechanical damage from the process, and temperature change may impact the rock and studs [4,15].

2.3. Laboratory-Based Methods for Dissolution

Laboratory-based approaches to investigating the dissolutional behaviors of carbonate rocks are important in that they allow for a deconvolution of factors at play during dissolution due to a controlled setting. Initial approaches at calculating the dissolution rates of carbonate rocks in the laboratory setting are based on the rotating disc principle, in which a sample is spun in water and the water is monitored to determine the dissolution rate based on the ions released from dissolution; Dreybrodt [9], and the references therein, provides an excellent overview of this technique. Numerous studies have since applied this rotating disc technique to calculate the dissolution rate of carbonate rocks (e.g., [18,19]). Other studies have used powdered rock samples instead of intact rock (e.g., [20–24]), whereas others have used intact rock samples and flowed water through/around the samples (e.g., [25–27]).

Several studies have investigated the role of petrology, petrography, and mineralogy on the dissolution rate of carbonate rocks, with the most common analysis attempting to distinguish between limestone and dolostone (e.g., [19,28,29]), dolostones and dolomite (e.g., [18]), and within various limestone types (e.g., [20–23,25]). Furthermore, it does appear that crystal face and orientation may also impact the dissolution rate of carbonate minerals (e.g., [29–31]). These studies have demonstrated that petrography, mineralogy, and crystal orientation does have a potentially significant impact on the dissolution rates of carbonates.

Many studies have attempted to quantify the dissolution kinetics of calcium carbonate as related to biotic and abiotic calcium carbonate (e.g., [23,32–37]). Cubillas et al. [23] report that biological calcium carbonate may have a slower dissolution rate, this appears to be due to biogenic carbonates containing organic matter.

The role that a sample's surface has on the dissolution rates of minerals has been discussed in the literature (e.g., [38–43]). The relative importance of modeling dissolution rates assuming an even diffusion boundary layer versus a more complicated surface (often defined by the Brunauer-Emmett-Teller theory (BET)) [40] is poorly constrained [38,39,41]. The preparation of carbonate samples to measure the BET may actually artificially inflate their surface area [23]. Levenson et al. [25] reported that in truly phreatic environments that perhaps only the nominal surface area of the sample is important when considering dissolution rates, but notes that this may not be accurate in the vadose environment. Pedrosa et al. [42] and Fischer et al. [43] provide an excellent overview of the role that

surface morphology contributes to the dissolution of rocks, ranging from roughness, grain size and distribution through boundary conditions.

It is important to note that across all of the reports discussed in this section that none of them consider how a rock as a whole will behave in the karstic dissolutional environment, therefore there still remains much work to be done to fully explore what role petrography has on the dissolution on carbonate rocks.

2.4. Dissolutional Mico-Textures

The development of micro-scale dissolution textures on carbonate rocks undergoing dissolution has advanced greatly in the last two decades. These micro-scale structures and features generally have the same shapes and patterns of larger, classical karren [44]. Several studies have viewed the mico-textural developments under scanning electron microscopy (SEM) (e.g., [20,23–25,45–47]), atomic force microscopy (e.g., [48,49]), and X-ray microtomography (e.g., [29,50,51]).

Polished rock surfaces may actually help to accelerate dissolution where the polished surface intersects a pore; this phenomenon may help to explain the often apparent disconnect between laboratory and field methods [48]. Furthermore, the mechanical removal of fine-grained carbonate minerals/allochems from a limestone may also accelerate the rates of overall weathering and help explain in part some of the differences between field observations and laboratory observations of carbonate rock dissolution rates [25,49].

General observations of these micro-textures have shown that in the cases where carbonate rocks have fine (micrite) and coarse (spar) calcite fractions that the finer fraction has preferentially dissolved, or been removed from the rock [20,51].

Much work remains to be done to evaluate the micro-textures that develop on whole carbonate rocks and the role that petrography has on developing preferential dissolutional features.

2.5. Climate Change

The role of karstic dissolution of carbonate rocks by carbonic acid has led to much discussion and debate about the relative importance of the process on the global carbon budget; Liu et al. [1] and Martin [2] provide an excellent overview of this discussion. It is well established that the dissolution of carbonate rocks by carbonic acid removes carbon dioxide from the atmosphere, at least on the short-term scale (e.g., [2,3,52–55]), the lingering question is what the ultimate fate of the bicarbonate ion may be and how long the carbon remains sequestered (e.g., [2,56,57]). Numerous studies have documented that the dissolution of carbonates does sequester carbon on relatively long-time scales (e.g., [58–62]). Yuan [53] demonstrated the potential impact of karstic dissolution as a mechanism to sequester carbon using an average denudation rate from around the world and applying it to all of the world's karst areas, he came up with a total of 6.08×10^8 tons/year of sequestered carbon due to karst processes. Gombert [52] demonstrated the potential impact of karst on the carbon budget using White's [12] theoretical maximum dissolution equation and came up with a total of 3×10^8 tons/year of sequestered carbon due to karst processes. While the total amount of carbon sequestered by karst processes may not represent a major component in the global carbon budget, it is nonetheless worth considering and noting as society deals with addressing and mitigating against anthropogenic climate change.

Several authors have also speculated on what role this karstic dissolution might have between the modern day and the last glacial maximum and how it may have impacted the start and end of the glacial cycles [63–66]. To complicate this issue of carbon dioxide and karstic processes, sulfuric acid, common in hypogene systems, may also be used for limestone dissolution, however its use results in the release of carbonate dioxide back into the atmosphere [2,56].

Much still remains to be done to determine what roles karstic processes exactly play in the global climate discussion, but there is little doubt that they do play a meaningful

part. This work seeks to add to that growing knowledge by reporting on how the relative dissolution rates of limestones by carbonic acid vary based on their petrography.

2.6. CO_2 Storage and Injection

In light of continued climate change, CO_2 has been injected into various carbonate reservoirs to sequester the carbon (e.g., [67–70]). These reservoirs are subsequently modified due to the presence of the CO_2 (e.g., [71–75]). Studies have demonstrated that the injection of CO_2 into these deep-seated reservoirs results in reorganization of the porosity and permeability of these units (e.g., [71–75]). The role of the petrology in this reorganization is poorly constrained, though based on a study by Seyyedi et al. [75], it appears that ooids preferentially dissolve relative to their surrounding cements. The work discussed in this paper may have implications for understanding how reservoirs that have been injected with CO_2 may respond and reorganize.

3. Methods

3.1. Samples Used

Two samples were analyzed for this project: oolitic limestone, and pentamerous limestone (dolostone). Calcite was previously used as a proof of concept for the experimental setup as described below [76]. The oolitic limestone was purchased from Ward's Science (part number 470026-100) and was collected from Bedford, IN, USA. The pentamerous limestone was also purchased from Ward's Science (part number 470026-070) and was collected from Rochester, NY, USA.

3.2. Sample Description

The oolitic limestone and pentamerous limestone were both described using standard petrographic techniques. Both samples were made into thin sections that were 30-µm thick and vacuum embedded with blue epoxy. Point counts using 100 random points across the slide were conducted using a mechanical stage on a Nikon Labophot-Pol. Representative photomicrographs of each limestone were taken using a Axiocam 105 camera mounted on the microscope.

Both rocks were also analyzed under powder x-ray diffraction (XRD) to determine their mineralogy. The powder XRD analysis was conducted on a Shimadzu Lab XRD-6100 at the University of Arkansas-Fort Smith. Samples were prepared in a mortar and pestle and ground until they easily passed through a 45 µm mesh. XRD patterns were obtained as follows: continuous mode, 0.020° per step, 2° 2 θ per minute, over 10–70° 2 θ, with CuKα radiation. While this XRD analysis describes only a small part of the rock it provides context for the general mineralogy of the rock.

3.3. Sample Preparation

One sample of each the oolitic and pentamerous limestone were cut down to ~2 cm cubes using a rock saw, dried for 24 h in a 100 °C oven, and then coated with marine epoxy. One side of each sample was hand polished using 150/220 mesh silicon carbide grit, followed by 600 mesh silicon carbide grit, and completed with 1000 mesh silicon carbide grit in preparation of the dissolution experiment. Samples were re-polished between each experimental replicate. The area of the polished surfaces was calculated from a high-resolution scan of the samples in ImageJ. Styrene bars were glued to the sides of the samples to hold them in the sample carrier using cyanoacetate glue.

3.4. Experimental Setup

The experimental setup described below is based roughly on the rotating sample experiments which has been modified as described below and in Leesburg et al. [77] and Emmons et al. [76] (Figure 1). A sample holder made of styrene was glued together using cyanoacetate to fit inside of a 1 L beaker and hold the rock sample. A 1-L beaker cover was cut to accept the sides of the sample holder and have three holes drilled into

it to accept: a fritted glass tube to supply CO_2, a conductivity probe, and a rubber cork that could be removed to collect discrete samples through a 5 mL volumetric pipette. The borosilicate beaker was filled to 800 mL with deionized water and placed on a stir plate and set to 200 rpm with the sample, sample holder, conductivity probe, and CO_2 supply in the beaker. CO_2 was released into the system at ~1 psi to ensure continued saturation of H_2CO_3 in the solution. Conductivity was recorded once every minute using a MicroLab FS-522. The conductivity probe was calibrated using six standards. Conductivity was used as a proxy for calcium ion concentration to allow for an approximate view of when the water began approaching saturation. The entire experimental apparatus was sealed with Parafilm at all of the seams to reduce evaporative loss and ensure a high CO_2 environment. The room where the experiments were conducted was held at a constant 20 °C. pH was not recorded with conductivity for these experiments because buffer solution leaks from pH probes under continued use and results in skewing of the conductivity data [76]. As CO_2 was constantly supplied, the water remained acidic over the length of the experiment. Prior work by Emmons et al. [76] demonstrated that the plastic used for the sample holders, styrene, do not dissolve over the timescales used in this project based on recorded conductivity.

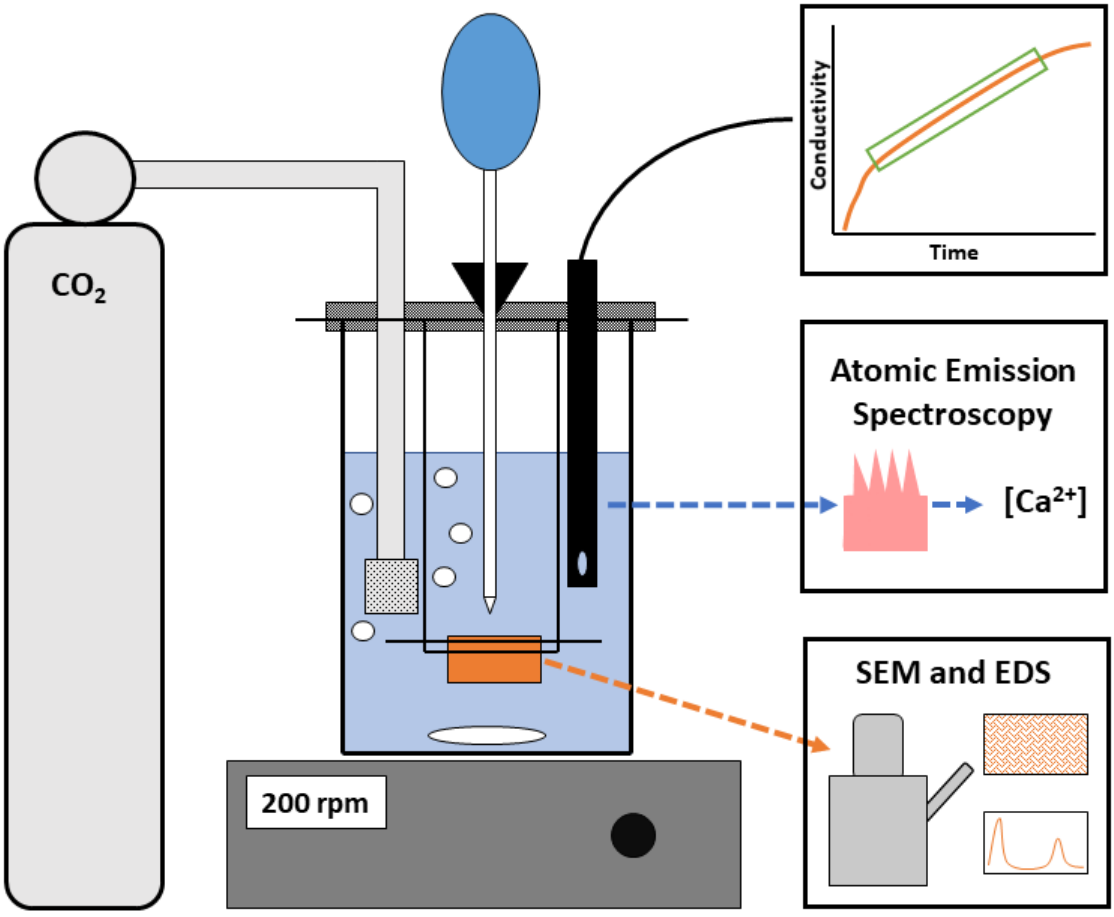

Figure 1. A diagrammatic representation of the experimental setup. Conductivity of the water was constantly monitored to determine when the water began approaching saturation. Discrete aliquots were collected and analyzed using atomic emission spectroscopy to determine the concentration of calcium in the water over time to calculate a dissolution rate. The rock samples were analyzed both pre- and post-dissolution on an SEM to determine if preferential dissolution was taking place. Refer to the text for more detailed information on the experimental setup.

Experiments were run until the slope of the conductivity of the sample water began to decrease, ensuring that the quickest rate of dissolution was captured by the experiments.

This meant each experiment ran for approximately 6000 min. Four runs of each experiment were conducted. 5 mL aliquots of water from the experimental setup were collected once every 360–720 min using a volumetric pipette and bulb. 5 mL of a fixative solution was also added to the collected water samples to ensure that the $CaCO_3$ did not precipitate out and to add KCl to the solution to reduce interference when conducting the atomic emission spectroscopy. The fixative solution contained 1 g of KCl and 10 mL of 12M HCl, dissolved in 990 mL of deionized water. The 50:50 mix of the sample and the fixative were stored at room temperature in labeled 4 dram borosilicate glass vials with a screw top lid lined with rubber until analysis via AES.

3.5. Atomic Emission Spectroscopy

Sample aliquots were analyzed on a Perkin-Elmer 2380 Atomic Absorption Spectrophotometer in emission mode using an acetylene-nitrous oxide flame set to a wavelength of 422.7 nm, with a 0.2 nm slit. All samples and calibration curves were run in random order in triplicate to account for instrument drift. The calcium calibration curve was created from five calcium standards.

3.6. Calculation of Dissolution Rates

Dissolution rates were calculated based on the line-of-best fit obtained for each sample using AES data. The data used for this calculation were the average of each experimental run for a given sample. The observed slope of each sample, initially expressed as the concentration of $[Ca]^{2+}$ per unit time, allowed the dissolution rate to be calculated using Equation (1) as previously described by Herman and White [18]:

$$Dissolution\ Rate = \frac{V}{A}\frac{dc}{dt} \quad (1)$$

where the volume of the solution (V), the surface area of the exposed rock (A), and the change in concentration of dissolved ions per unit time (dc/dt) permits the calculation of dissolution rate. Furthermore, expressing both these results and the density of the sample in molar concentrations, dissolution rate per a period unit of time is easily calculated (further calculations can be found in Supplementary Material, Table S1). While at first glance the use of only $[Ca]^{2+}$ concentration data allows the dissolution rate of limestone to be calculated, the difference of the slopes obtained between calcium concentration and conductivity can be used to approximate the relative abundance of other ions and help the distinction between limestone and dolostone.

3.7. Scanning Electron Microscopy

Both sets of samples were viewed under a SEM. The JOEL JSM-7200F Field Emission SEM at Marshall University's Imaging Core was used for this analysis. Two samples of the oolitic and pentamerous limestone were each viewed under the SEM, one sample each pre-dissolution and one sample each post-dissolution to determine if there was any preferential dissolution happening within the two limestones. All samples were sonicated in 99% ethanol for 10 min and oven dried before being placed in the SEM to remove any contaminants from their surface. Samples were attached to a stainless-steel stub using carbon tape; they did not receive a sputter coating. They were viewed at magnifications from 40×–1000× at 3.0 kV.

4. Results

4.1. Sample Descriptions

4.1.1. Oolitic Limestone

Based on the petrographic analysis the oolitic limestone is a grainstone/sorted oosparite (Figure 2). Point count analysis (n = 100) determined that the rock was in order of relative abundance: 61% ooids/coated grains, 17% calcite spar, 11% foraminifera, 6% porosity, 5% brachiopod, and 1% trilobite. XRD analysis determined that the rock is 100% calcite.

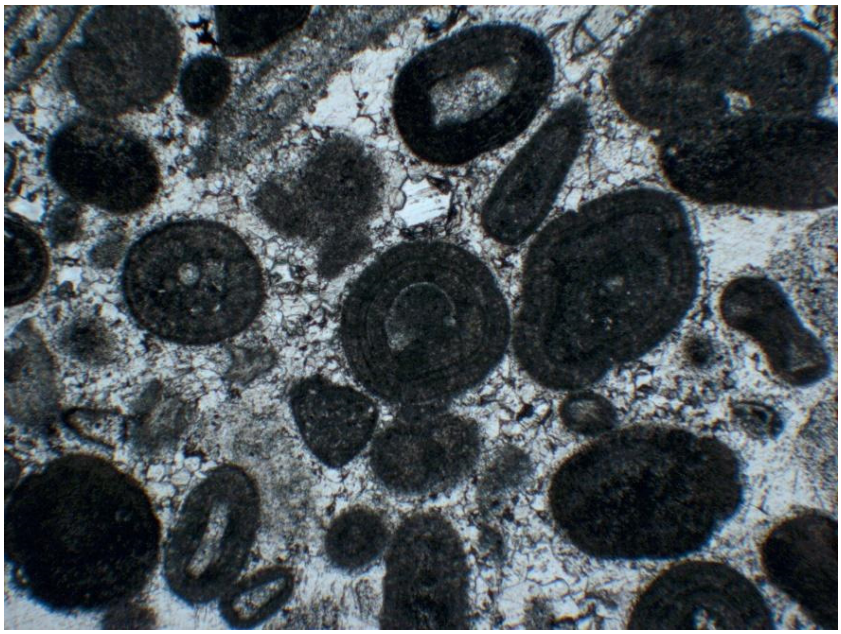

Figure 2. A representative photomicrograph of the oolitic limestone in plane-polarized light. The width of the photomicrograph is 3 mm.

4.1.2. Pentamerous Limestone (Dolostone)

Based on petrographic analysis the pentamerous limestone (dolostone) is a dolograinstone/unsorted biodolosparite (Figure 3). Point count analysis (n = 100) determined that the rock was, in order of relative abundance: 61% brachiopod, 21% spar, 16% echinoderm, and 2% porosity. XRD analysis determined that the rock is approximately 72% dolomite, and 27% calcite, with 1% quartz, because the official name of the sample from Ward's Science is Pentamerous Limestone this paper will continue referring to it in that way with a parenthetical note that it is actually a dolostone.

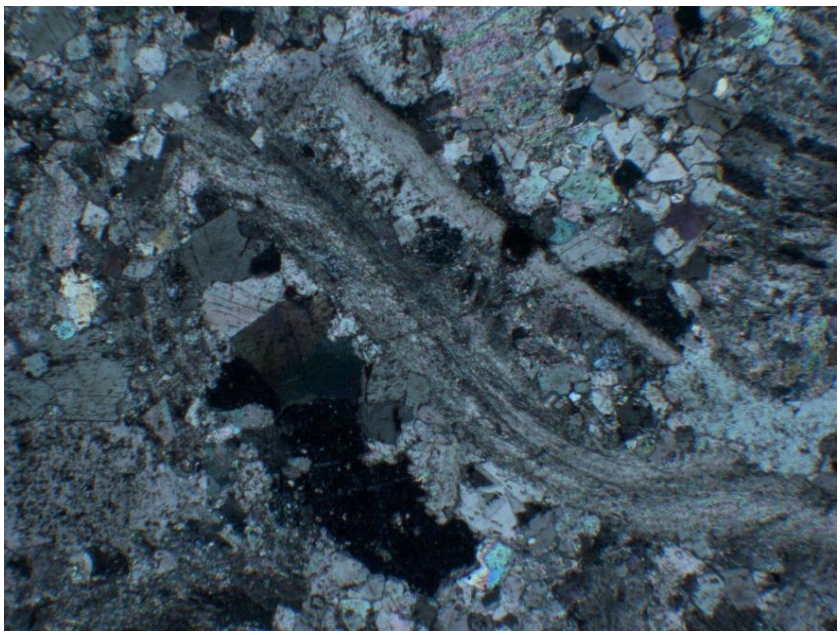

Figure 3. A representative photomicrograph of the pentamerous limestone (dolostone) in cross-polarized light. The width of the photomicrograph is 3 mm.

4.2. Dissolution Rates

4.2.1. Oolitic Limestone

The oolitic limestone in this study exhibited a rather fast dissolution rate of 1579 cm/Kyr, the dissolved sample quickly reaching equilibrium at approximately 6000 min (Figure 4A). In the laboratory scale without extrapolation, this value could be viewed as approximately 0.0018 mm removed from the sample surface per hour. Experimentally, it was observed that it takes ~120 min, given the described method for reproducible and quantitative data to be observed as the water becomes saturated with H_2CO_3; the initial dissolution kinetics shown in Figure 4B. Both conductivity data and calcium concentration data (Figure 4C) demonstrate good agreement on the dissolution kinetics of the sample, as the comparative slopes between samples are similar using both types of data. The reproducibility of the obtained slopes between each experiment was found to be approximately 19.3 relative standard deviation percent (RSD) in regards to calcium concentration and only 9.2 RSD for conductivity data. Results for individual experimental replicates for both calcium ion and conductivity data can be found in Supplementary Material, Figures S1 and S2, respectively.

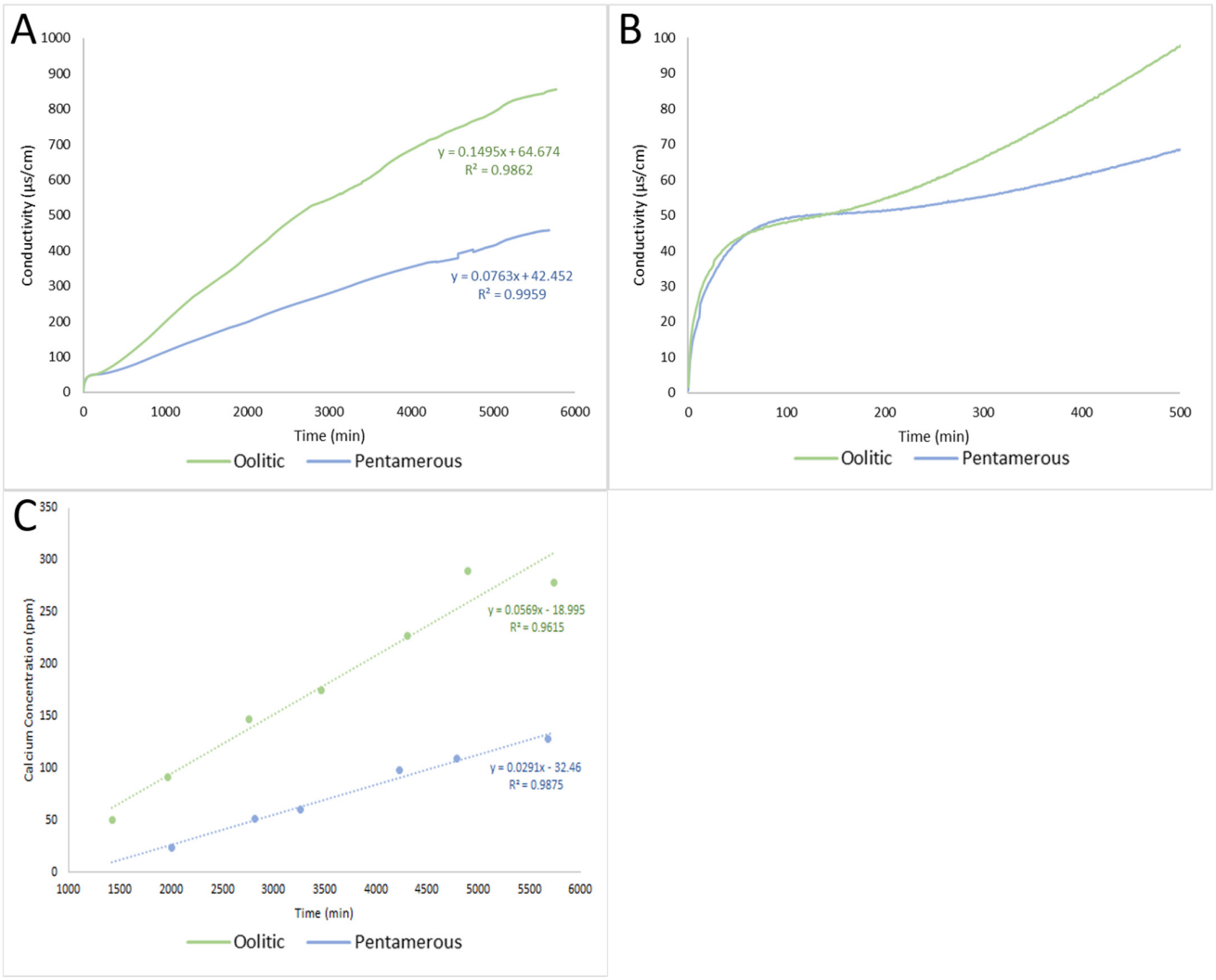

Figure 4. Dissolution data obtained through the course of the experiment demonstrating (**A**) conductivity over time, (**B**) conductivity at the start of the experiment and (**C**) calcium concentration data. The individual trial data can be found in the Supplemental Materials.

4.2.2. Pentamerous Limestone (Dolostone)

In comparison to the previously mentioned oolitic limestone, the pentamerous sample exhibited a far lower dissolution rate of 799 cm/Kyr, this being 0.00091 mm per hour. The initial dissolution kinetics remained similar at ~120 min, however, at only ~180 min there was a significant difference in dissolution rates, with the pentamerous limestone dissolving at a much lower rate (Figure 4A,B). Reproducibility for these experiments in reference to calcium concentration and conductivity data was 17.2 and 4.2 RSD, respectively. Results for individual experimental replicates for both calcium ion and conductivity data can be found in Supplementary Material, Figures S3 and S4, respectively. Figures of merit associated with both samples along with data used in their dissolution calculations are summarized in Table 1.

Table 1. Summary of all dissolution data obtained with both limestone samples and their respective figures of merit.

Sample	Density (g/cm^3)	Surface Area (cm^2)	Denudation Rate (cm/Kyr)	Absolute Error (cm/Kyr)	Ca^{2+} Slope (ppm/min)	Conductivity Slope ((µs/cm)/min)	Ca^{2+} RSD %	Conductivity RSD %
Oolitic	2.71	5.495	1579	305	0.056	0.1495	19.3	9.2
Pentamerous	2.81	4.855	799	137	0.026	0.0763	17.2	4.2

4.3. Micro-Textures

4.3.1. Oolitic Limestone

The oolitic limestone was polished before the experiment and analyzed under SEM (Figure 5A). The sample pre-dissolution was a smooth, texture-less surface, with the exception of the minimal porosity in the rock. After dissolution in the experimental apparatus for ~6000 min the sample developed a complicated surface texture (Figure 5B,C). It appears from the photomicrographs that the ooids preferentially dissolved during the experiment, while leaving the cements in positive relief. The cements did dissolve given their textures, however not to the same degree that the ooids did.

4.3.2. Pentamerous Limestone (Dolostone)

The pentamerous limestone (dolostone) was polished before the experiment and analyzed under SEM (Figure 5D). The sample pre-dissolution was a smooth, texture-less surface. After dissolution in the experimental apparatus for ~6000 min the sample developed a complicated surface texture (Figure 5E,F). It appears from the photomicrographs that the brachiopods in the samples dissolved slightly more so than the surrounding matrix of the rock. It also appears that some of the matrix may have been physically/mechanically removed from the sample given the euhedral crystal faces; when physically handling the samples after dissolving, it was possible to feel some silt-sized grains come off of the rock.

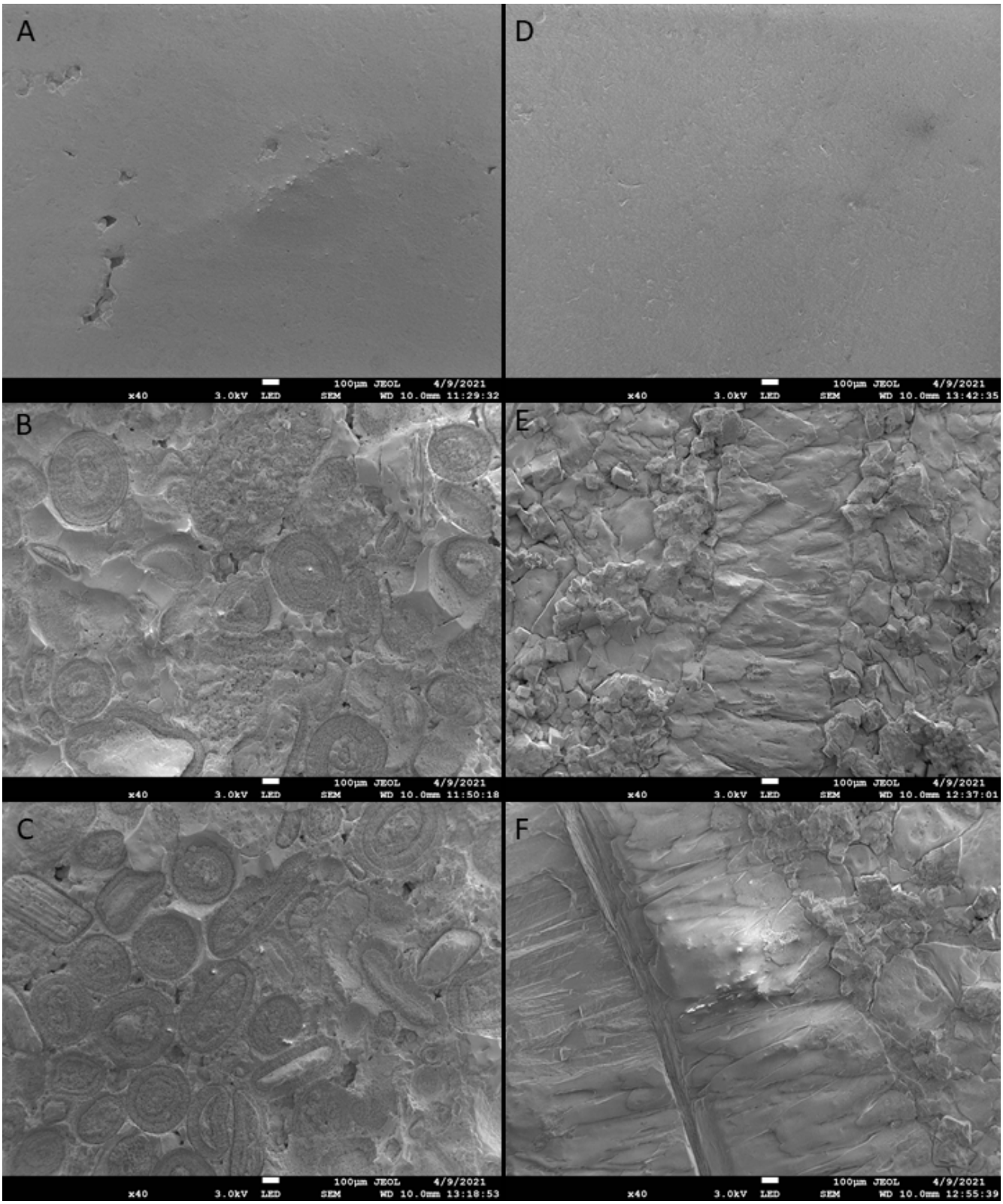

Figure 5. Representative SEM photomicrographs of the oolitic and pentarmerous rocks, pre- and post-dissolution. (**A**) Pre-dissolutional textures of the oolitic limestone. (**B**,**C**) Post-dissolutional textures of the oolitic limestone. (**D**) Pre-dissolutional textures of the pentamerous limestone (dolostone). (**E**,**F**) Post-dissolutional textures of the pentamerous limestone (dolostone).

5. Discussion

5.1. Dissolution Rates

The controlled nature of the described approach and the reduction of extraneous variables associated with field-studies allowed considerably high amounts of reproducibility between experiments to be obtained. This rugged approach gives reliable and applicatory dissolution data which have direct bearing on acid-associated carbonate dissolution. Moreover, the cost-effectiveness and throughput of this approach can enable the further modeling of carbonate dissolution in a variety of different samples. Experimental dissolution rates of both the oolitic and pentamerous limestones are, as one would expect, higher than values obtained by other methods (e.g., [4,52]) due to the constant influx of CO_2. In comparison to a similar approach by Martinez and White [28], which also had constant saturation of CO_2, observed results are within the same order of magnitude. However, as this technique allows rapid results with highly reproducible data, relative dissolution rates between samples can be readily documented. The absolute dissolution rate of the oolitic limestone sample, 1579 cm/Kyr, is far higher than the real-world 100′s of mm/Kyr scale commonly found in theoretical and field calculations. This data, however, compared to dissolution rates that are gathered on the field or samples processed with the same method, allow relative dissolution rates to be calculated without prohibitive instrumentation.

A comparison of the oolitic and pentamerous limestones demonstrates that calcium dissolution for the oolitic sample was almost twice as fast as the pentamerous sample, 98% faster. Moreover, conductivity data reveal that the oolitic limestone sample dissolved approximately 96% faster, with great agreement with the data obtained by AES. These results suggest that even limestones with higher amounts of dolomite (in the case of the pentamerous limestone) can have accurate relative dissolution rates calculated with only the use of a conductivity probe. As previous reports have suggested field reports exceeding 600 µm/cm under highly carbonated waters [78], the results obtained in this experiment are in line with real-world conditions.

5.2. Micro-Textures

Both the carbonate rocks started with a featureless surface prior to dissolution (Figure 5A,D). Both samples picked up complicated textures following ~6000 min of dissolution in the experiment (Figure 5B,C,E,F). In the case of the oolitic limestone it appears that all fabrics in the rock dissolved, however the ooids seemed to dissolve preferentially to the matrix of the rock. In most of the ooids their core was in positive relief suggesting that the core was less dissolvable than the coatings. The coatings of the ooids themselves are made of fine-grained carbonates (e.g., [79]) allowing for a possible increase in surface area for dissolution or for possible mechanical weathering of the material [49,80].

In the pentamerous limestone (dolostone) it appears that all of the fabrics dissolved. The brachiopods themselves appear to have dissolved significantly whereas the surrounding matrix does not appear to have dissolved as much. However, it does appear that there may have been some mechanical weathering of the matrix in the rock given the euhedral crystal faces. This mechanical/physical weathering superimposed on the dissolution of the rock can be significant [49,80]. It was possible to physically feel some of the silt-sized grains come free from the sample when handling it post-dissolution.

The SEM imagery of the samples was useful to determine that the two samples investigated in this study did not dissolve uniformly from a polished surface. It appears that the allochems in the rocks preferentially dissolved (brachiopods and ooids), while the cement and matrix did not dissolve as readily.

5.3. Implications

Prior studies looking at the dissolution rates of carbonates focus on rock powders or have not focused on what is happening between the constituent components of the rock. This study documents that at least these two rocks do not dissolve evenly across their surface, apparently due to their fabric make-up and in the case of the pentamerous

rock, perhaps differences in their mineralogy. The role of mechanical weathering at the micro-scale in the dissolution of carbonate rocks cannot be discounted and should be explored greater in the future.

This has significant implications for understanding the dissolution rates of carbonate rocks, both from a denudation/weathering perspective and a climate perspective. Understanding the denudation and dissolution rates of carbonates is important to understanding cave, karst, and landscape evolution. Cave and karst studies typically ignore the role of petrology and petrography on the formation of karst, this small-scale laboratory experiment suggests that it may be important to consider.

Climatic studies have focused on the role of the dissolution of carbonate rocks on the global carbon budget—there is little doubt that it plays an important role (e.g., [2]). The next step to take in looking at the carbon budget and carbonate dissolution is what role petrology, petrography, and mineralogy has on the amount of carbon sequestered. Larson and Mylroie [63] speculated on the importance of calcite versus aragonite dissolution in sequestering carbon, but there remains much to be determined looking at other carbonate minerals and the petrography of the rocks.

The importance of the method and procedure described in this paper is significant as it allows for the understanding of rock dissolving processes by controlling for them in a lab setting. The lab setting may not match the real world perfectly, but it provides for a way to control the system. Furthermore, this paper reports that the methods and procedures described within it work for both limestone and dolostone opening the way for additional studies. It is critical that an experimental design for carbonate dissolution to be inexpensive, reproducible, and timely to allow future studies to better access relative carbonate dissolution across a variety of samples and localities. There remains much work to be continued investigating the behavior of the dissolution of whole carbonate rocks both from the perspective of total dissolution rates and the micro-textures developed during dissolution which suggest differential dissolution/weathering.

5.4. Future Considerations

Future investigations need to further document the role that petrography and mineralogy has on the dissolution of limestone. This study is a preliminary attempt at that to document that the petrography does seem to be important on the dissolution rates of limestones through whole rock dissolution experiments. Carbonate rocks of additional petrographic makeup, age, and mineralogy need to be analyzed to determine if the observations in this report continue to hold as to the relative dissolution rates and textures developed. Moreover, the additional analysis of different ionic species (e.g., magnesium) could also provide insight on the differential dissolution observed between samples. It would also be useful to place these samples in the field environment as rock-tablets (e.g., [13,14]) and compare the rates of dissolution and the differential textures developed and if they are similar, this would be useful in documenting how significant of a role the petrology, petrography, and mineralogy of carbonate rocks have on the global carbon budget outside of a laboratory setting.

6. Conclusions

Determining the dissolution rate of carbonate rocks is important to our understanding of cave, karst, and landscape processes along with understanding of the global carbon budget. This study reports that the petrography and mineralogy of carbonate rocks does impact their dissolution rate in the laboratory setting. Furthermore, this work demonstrates that not all of the constituent parts of carbonate rocks dissolve evenly and that there may also be some mechanical/physical weathering happening around the grains, all suggesting that the carbonate rock petrography may be more important in understanding karst processes than commonly considered by karst researchers. Laboratory dissolution experiments are important in that they allow for a deconvolution of factors controlling the dissolution of carbonate rocks, while this method was also demonstrated to work with both

limestone and dolostone. Much work remains to be done to determine if the observations in this study exist in the natural environment and what relative importance they play in the development of karst and global carbon budget.

Supplementary Materials: The following are available online at https://www.mdpi.com/article/10.3390/min11060605/s1. Table S1: Calculation steps needed to use the data described in text to perform denudation rate calculations. Figure S1: Experimental replicates of the oolitic limestone sample utilizing AES. Figure S2: Conductivity data for all experimental replicates of the oolitic limestone sample. Figure S3: AES results from all experimental replicates of pentamerous limestone (dolostone). Figure S4: Conductivity for all experimental replicates of the pentamerous limestone (dolostone) sample.

Author Contributions: Conceptualization, data curation, writing—review and editing: E.B.L. and R.V.E. All authors have read and agreed to the published version of the manuscript.

Funding: This research received no external funding.

Data Availability Statement: Data generated in this study can be found in the Supplemental Materials or by contacting the authors.

Acknowledgments: The authors thank Daniel Finnen and Andrew Napper for discussions about experimental setup and help with the spectrometer. Blake Smalley is thanked for helping to run the samples on the spectrometer and the SEM. Jessica Leesburg and V. Peyton Hall are thanked for their help in the early parts of this project. Maurice Testa at the University of Arkansas-Fort Smith is thanked for running the samples on the XRD. David Neff at Marshall University is thanked for his help with the SEM analysis. Shawnee State University is also thanked for funding this project. Finally, the authors thank three anonymous reviewers whose comments improved the quality of the paper.

Conflicts of Interest: The authors declare no conflict of interest.

References

1. Liu, Z.; Macpherson, G.; Groves, C.; Martin, J.B.; Yuan, D.; Zeng, S. Large and active CO_2 uptake by coupled carbonate weathering. *Earth-Sci. Rev.* **2018**, *182*, 42–49. [CrossRef]
2. Martin, J.B. Carbonate minerals in the global carbon cycle. *Chem. Geol.* **2017**, *449*, 58–72. [CrossRef]
3. Ford, D.C.; Williams, P.W. *Karst Hydrogeology and Geomorphology*; Wiley: Chichester, UK, 2007.
4. Gabrovšek, F. On concepts and methods for the estimation of dissolutional denudation rates in karst areas. *Geomorphology* **2009**, *106*, 9–14. [CrossRef]
5. White, W.B. *Geomorphology and Hydrology of Karst Terrains*; Oxford: New York, NY, USA, 1988.
6. Corbel, J. Érosion en terrain calcaire (Vitesse d'érosion et morhologie). *Ann. Geogr.* **1959**, *68*, 97–120. [CrossRef]
7. Jakucs, L. *Morphogenetics of Karst Regions: Variants of Karst Evolution*; Wiley: New York, NY, USA, 1977.
8. Trudgill, S. Classics in physical geography revisited: Corbel, J. 1959: Érosion en terrain calcaire (Vitesse d'érosion et morhologie). *Annales de Géographie* 68, 97–120. *Progr. Phys. Geogr.* **2008**, *32*, 684–690.
9. Dreybrodt, W. *Processes in Karst Systems: Physics, Chemistry, and Geology*; Springer: Berlin, Germany, 1988.
10. Morse, J.W.; Arvidson, R. The dissolution kinetics of major sedimentary carbonate minerals. *Earth-Sci. Rev.* **2002**, *58*, 51–84. [CrossRef]
11. Morse, J.W.; Arvidson, R.; Lüttge, A. Calcium Carbonate Formation and Dissolution. *Chem. Rev.* **2007**, *107*, 342–381. [CrossRef]
12. White, W.B. Rate Processes: Chemical kinetics and karst landform development. In *Groundwater as a Geomorphic Agent*; LaFleur, R.G., Ed.; Allen and Unwin: Boston, MA, USA, 1984; pp. 227–248.
13. Trudgill, S.T. Measurement of erosional weight-loss of rock tablets. In *British Geomorphological Research Group Technical Bulleting No. 17*; Shorter Technical Methods (I); Brunsden, D., Thornes, J.B., Eds.; British Geomorphological Research Group: Sheffield, UK, 1975; pp. 13–19.
14. Krklec, K.; Domínguez-Villar, D.; Perica, D. Use of rock tablet method to measure rock weathering and landscape denudation. *Earth-Sci. Rev.* **2021**, *212*, 103449. [CrossRef]
15. Moses, C.; Robinson, D.; Barlow, J. Methods for measuring rock surface weathering and erosion: A critical review. *Earth-Sci. Rev.* **2014**, *135*, 141–161. [CrossRef]
16. Stephenson, W.; Finlayson, B. Measuring erosion with the micro-erosion meter—Contributions to understanding landform evolution. *Earth-Sci. Rev.* **2009**, *95*, 53–62. [CrossRef]
17. Inkpen, R. Errors in measuring the percentage dry weight change of stone tablets. *Earth Surf. Process. Landf.* **1995**, *20*, 783–793. [CrossRef]

18. Herman, J.S.; White, W.B. Dissolution kinetics of dolomite: Effects of lithology and fluid flow velocity. *Geochim. Cosmochim. Acta* **1985**, *49*, 2017–2026. [CrossRef]
19. Liu, Z.; Yuan, D.; Dreybrodt, W. Comparative study of dissolution rate-determining mechanisms of limestone and dolomite. *Environ. Earth Sci.* **2005**, *49*, 274–279. [CrossRef]
20. Kirstein, J.; Hellevang, H.; Haile, B.G.; Gleixner, G.; Gaupp, R. Experimental determination of natural carbonate rock disso-lution rates with a focus on temperature dependency. *Geomorphology* **2016**, *261*, 30–40. [CrossRef]
21. Shih, S.-M.; Lin, J.-P.; Shiau, G.-Y. Dissolution rates of limestones of different sources. *J. Hazard. Mater.* **2000**, *79*, 159–171. [CrossRef]
22. Pracný, P.; Faimon, J.; Všianský, D.; Přichystal, A. Evolution of Mg/Ca and Sr/Ca ratios during the experimental dissolution of limestone. *Chem. Geol.* **2019**, *523*, 107–120. [CrossRef]
23. Cubillas, P.; Köhler, S.; Prieto, M.; Chaïrat, C.; Oelkers, E.H. Experimental determination of the dissolution rates of calcite, aragonite, and bivalves. *Chem. Geol.* **2005**, *216*, 59–77. [CrossRef]
24. Järvinen, L.; Leiro, J.A.; Bjondahl, F.; Carletti, C.; Eklund, O. XPS and SEM study of calcite bearing rock powders in the case of reactivity measurement with HCl solution. *Surf. Interface Anal.* **2011**, *44*, 519–528. [CrossRef]
25. Levenson, Y.; Schiller, M.; Kreisserman, Y.; Emmanuel, S. Calcite dissolution rates in texturally diverse calcareous rocks. *Geol. Soc. Lond. Spéc. Publ.* **2015**, *406*, 81–94. [CrossRef]
26. Luquot, L.; Rodriguez, O.; Gouze, P. Experimental Characterization of Porosity Structure and Transport Property Changes in Limestone Undergoing Different Dissolution Regimes. *Transp. Porous Media* **2014**, *101*, 507–532. [CrossRef]
27. Sterpenich, J.; Sausse, J.; Pironon, J.; Géhin, A.; Hubert, G.; Perfetti, E.; Grgic, D. Experimental ageing of oolitic limestones under CO_2 storage conditions petrographical and chemical evidence. *Chem. Geol.* **2009**, *265*, 99–112. [CrossRef]
28. Martinez, M.I.; White, W.B. A laboratory investigation of the relative dissolution rates of the Lirio Limestone and the Isla de Mona Dolomite and the implications for cave and karst development on Isla de Mona. *J. Cave Karst Stud.* **1999**, *61*, 7–12.
29. Noiriel, C.; Bernard, D.; Gouze, P.; Thibault, X. Hydraulic Properties and Microgeometry Evolution Accompanying Limestone Dissolution by Acidic Water. *Oil Gas. Sci. Technol.* **2005**, *60*, 177–192. [CrossRef]
30. Lea, A.; Amonette, J.; Baer, D.; Liang, Y.; Colton, N. Microscopic effects of carbonate, manganese, and strontium ions on calcite dissolution. *Geochim. Cosmochim. Acta* **2001**, *65*, 369–379. [CrossRef]
31. Liang, Y.; Baer, D.R. Anisotropic dissolution at the CaCO3 (1014)-water interface. *Surf. Sci.* **1997**, *373*, 275–287. [CrossRef]
32. Kier, R.S. The dissolution kinetics of biogenic calcium carbonates in seawater. *Geochim. Cosmochim. Acta* **1980**, *44*, 241–252. [CrossRef]
33. Norzagaray-López, O.C.; Calderon-Aguilera, L.E.; Castro-Ceseña, A.B.; Hirata, G.; Hernandez-Ayon, J.M. Skeletal dissolution kinetics and mechanical tests in response to morphology among coral genera. *Facies* **2017**, *63*, 7. [CrossRef]
34. Pickett, M.; Anderson, A.J. Dissolution rates of biogenic carbonates in natural seawater at different pCO2 conditions: A la-boratory study. *Aquat. Geochem.* **2015**, *21*, 459–485. [CrossRef]
35. Walter, L.M.; Morse, J.W. Magnesian calcite stabilities: A reevaluation. *Geochim. Cosmochim. Acta* **1984**, *48*, 1059–1069. [CrossRef]
36. Walter, L.M.; Morse, J.W. Reactive surface area of skeletal carbonates during dissolution: Effect of grain size. *J. Sediment. Petrol.* **1984**, *54*, 1081–1090.
37. Walter, L.M.; Morse, J.W. The dissolution kinetics of shallow marine carbonates in seawater: A laboratory study. *Geochim. Cosmochim. Acta* **1985**, *49*, 1503–1513. [CrossRef]
38. Fischer, C.; Arvidson, R.; Lüttge, A. How predictable are dissolution rates of crystalline material? *Geochim. Cosmochim. Acta* **2012**, *98*, 177–185. [CrossRef]
39. Jeschke, A.A.; Dreybrodt, W. Dissolution rates of minerals and their relation to surface morphology. *Geochim. Cosmochim. Acta* **2002**, *66*, 3055–3062. [CrossRef]
40. Brunauer, S.; Emmett, P.H.; Teller, E. Adsorption of Gases in Multimolecular Layers. *J. Am. Chem. Soc.* **1938**, *60*, 309–319. [CrossRef]
41. Sing, K.S. Adsorption methods for the characterization of porous materials. *Adv. Colloid Interface Sci.* **1998**, *76–77*, 3–11. [CrossRef]
42. Pedrosa, E.T.; Kurganskaya, I.; Fischer, C.; Luttge, A. A Statistical Approach for Analysis of Dissolution Rates Including Surface Morphology. *Minerals* **2019**, *9*, 458. [CrossRef]
43. Fischer, C.; Kurganskaya, I.; Schäfer, T.; Lüttge, A. Variability of crystal surface reactivity: What do we know? *Appl. Geochem.* **2014**, *43*, 132–157. [CrossRef]
44. Viles, H.A.; Moses, C.A. Experimental production of weathering nanomorphologies on carbonate stone. *Q. J. Eng. Geol. Hydrogeol.* **1998**, *31*, 347–357. [CrossRef]
45. Moses, C.; Spate, A.P.; Smith, D.I.; Greenaway, M.A. Limestone weathering in Eastern Australia Part 2: Surface micromor-phology study. *Earth Surf. Process. Landf.* **1995**, *20*, 501–514. [CrossRef]
46. Zhang, Y.; Tian, W.; Qu, X.; Gao, S.; Chen, S.; How, L.F. Water-Rock Simulation During Limestone Dissolution. *J. Eng. Sci. Technol. Rev.* **2019**, *12*, 51–59. [CrossRef]
47. Levenson, Y.; Ryb, U.; Emmanuel, S. Comparison of field and laboratory weathering rates in carbonate rocks from an Eastern Mediterranean drainage basin. *Earth Planet. Sci. Lett.* **2017**, *465*, 176–183. [CrossRef]
48. Levenson, Y.; Emmanuel, S. Pore-scale heterogeneous reaction rates on a dissolving limestone surface. *Geochim. Cosmochim. Acta* **2013**, *119*, 188–197. [CrossRef]

49. Levenson, Y.; Emmanuel, S. Quantifying micron-scale grain detachment during weathering experiments on limestone. *Geochim. Cosmochim. Acta* **2016**, *173*, 86–96. [CrossRef]
50. Noiriel, C.; Gouze, P.; Bernard, D. Investigation of porosity and permeability effects from microstructure changes during limestone dissolution. *Geophys. Res. Lett.* **2004**, *31*, 24603. [CrossRef]
51. Noiriel, C.; Luquot, L.; Madé, B.; Raimbault, L.; Gouze, P.; van der Lee, J. Changes in reactive surface area during limestone dissolution: An experimental and modelling study. *Chem. Geol.* **2009**, *265*, 160–170. [CrossRef]
52. Gombert, P. Role of karstic dissolution in global carbon cycle. *Glob. Planet. Chang.* **2002**, *33*, 177–184. [CrossRef]
53. Yuan, D. The carbon cycle in karst. *Z. Geomorphol.* **1997**, *180*, 91–102.
54. Liu, Z.; Dreybrodt, W.; Liu, H. Atmospheric CO_2 sink: Silicate weathering or carbonate weathering? *Appl. Geochem.* **2011**, *26*, S292–S294. [CrossRef]
55. Cao, J.-H.; Wu, X.; Huang, F.; Hu, B.; Groves, C.; Yang, H.; Zhang, C.-L. Global significance of the carbon cycle in the karst dynamic system: Evidence from geological and ecological processes. *China Geol.* **2018**, *1*, 17–27. [CrossRef]
56. Martin, J.B.; Brown, A.; Ezell, J. Do carbonate karst terrains affect the global carbon cycle? *Acta Carsol.* **2013**, *42*, 187–196. [CrossRef]
57. Gaillardet, J.; Calmels, D.; Romero-Mujalli, G.; Zakharova, E.; Hartmann, J. Global climate control on carbonate weathering intensity. *Chem. Geol.* **2019**, *527*, 118762. [CrossRef]
58. Zhou, G.; Jia, B.; Tao, X.; Yan, H. Estimation of karst carbon sink and its contribution to CO_2 emissions over a decade using remote sensing imagery. *Appl. Geochem.* **2020**, *121*, 104689. [CrossRef]
59. Jiang, Z.; Lian, Y.; Qin, X. Carbon cycle in the epikarst systems and its ecological effects in South China. *Environ. Earth Sci.* **2013**, *68*, 151–158. [CrossRef]
60. Liu, Z.; Zhao, J. Contribution of carbonate rock weathering to the atmospheric CO 2 sink. *Environ. Earth Sci.* **2000**, *39*, 1053–1058. [CrossRef]
61. Liu, Z.; Dreybrodt, W.; Wang, H. A new direction in effective accounting for the atmospheric CO_2 budget: Considering the combined action of carbonate dissolution, the global water cycle and photosynthetic uptake of DIC by aquatic organisms. *Earth-Sci. Rev.* **2010**, *99*, 162–172. [CrossRef]
62. Cao, J.; Hu, B.; Groves, C.; Huang, F.; Yang, H.; Zhang, C.; Jianhua, C.; Bill, H.; Chris, G.; Fen, H.; et al. Karst dynamic system and the carbon cycle. *Z. Geomorphol. Suppl. Issues* **2016**, *60*, 35–55. [CrossRef]
63. Larson, E.B.; Mylroie, J.E. Quaternary glacial cycles: Karst processes and the global CO_2 budget. *Acta Carsol.* **2013**, *42*, 197–202. [CrossRef]
64. Ludwig, W.; Amiotte-Suchet, P.; Munhoven, G.; Probst, J.-L. Atmospheric CO_2 consumption by continental erosion: Present day controls and implications for the last glacial maximum. *Glob. Planet. Chang.* **1998**, *16–17*, 107–120. [CrossRef]
65. Mylroie, J.E. Carbonate deposition/dissolution cycles and carbon dioxide flux in the Pleistocene. In *Proceedings of the Sixth Symposium on the Geology of the Bahamas, San Salvador, Bahamas, January 1993*; White, B., Ed.; Bahamian Field Station: San Salvador, The Bahamas, 1993; pp. 103–107.
66. Mylroie, J.E. Late Quaternary sea-level position: Evidence from Bahamian carbonate deposition and dissolution cycles. *Quat. Int.* **2008**, *183*, 61–75. [CrossRef]
67. Kelemen, P.; Benson, S.M.; Pilorgé, H.; Psarras, P.; Wilcox, J. An Overview of the Status and Challenges of CO_2 Storage in Minerals and Geological Formations. *Front. Clim.* **2019**, *1*, 9. [CrossRef]
68. Raza, A.; Gholami, R.; Rezaee, R.; Bing, C.H.; Nagarajan, R.; Hamid, M.A. Preliminary assessment of CO_2 injectivity in car-bonate storage sites. *Petroleum* **2017**, *3*, 144–154. [CrossRef]
69. Raza, A.; Gholami, R.; Rezaee, R.; Bing, C.H.; Nagarajan, R.; Hamid, M.A. Preliminary assessments of CO_2 storage in carbonate formations: A case study from Malaysia. *J. Geophys. Eng.* **2017**, *14*, 533–554. [CrossRef]
70. Siqueria, T.A.; Iglesias, R.S.; Ketzer, J.M. Carbon dioxide injection in carbonate reservoirs—A review of CO_2-water-rock interaction studies. *Greenh. Gases Sci. Technol.* **2017**, *7*, 1–14.
71. Luquot, L.; Gouze, P. Experimental determination of porosity and permeability changes induced by injection of CO_2 into carbonate rocks. *Chem. Geol.* **2009**, *265*, 148–159. [CrossRef]
72. Gharbi, O.; Bijeljic, B.; Boek, E.; Blunt, M. Changes in Pore Structure and Connectivity Induced by CO_2 Injection in Carbonates: A Combined Pore-Scale Approach. *Energy Procedia* **2013**, *37*, 5367–5378. [CrossRef]
73. Singh, K.; Anabaraonye, B.U.; Blunt, M.; Crawshaw, J. Partial dissolution of carbonate rock grains during reactive CO_2-saturated brine injection under reservoir conditions. *Adv. Water Resour.* **2018**, *122*, 27–36. [CrossRef]
74. Elkhoury, J.E.; Ameli, P.; Detwiler, R.L. Dissolution and deformation in fractured carbonates caused by flow of CO_2-rich brine under reservoir conditions. *Int. J. Greenh. Gas. Control.* **2013**, *16*, S203–S215. [CrossRef]
75. Seyyedi, M.; Ben Mahmud, H.K.; Verrall, M.; Giwelli, A.; Esteban, L.; Ghasemiziarani, M.; Clennell, B. Pore Structure Changes Occur During CO_2 Injection into Carbonate Reservoirs. *Sci. Rep.* **2020**, *10*, 1–14. [CrossRef]
76. Emmons, R.; Finnen, D.; Larson, E. A laboratory method for measuring carbonate dissolution rates. In Proceedings of the Geological Society of America Annual Meeting, Indianapolis, IN, USA, 4–7 November 2017.
77. Leesburg, J.N.; Hall, V.P.; Larson, E.B. Calculating Denudation Rates of Carbonate Rocks: A New Laboratory Method. In Proceedings of the Geological Society of America Annual Meeting, Denver, CO, USA, 25–28 September 2016; Denver, CO, USA, 2016.

78. Krawczyk, W.E.; Ford, D.C. Correlating specific conductivity with total hardness in limestone and dolomite karst waters. *Earth Surf. Process. Landf.* **2006**, *31*, 221–234. [CrossRef]
79. Simone, L. Ooids: A review. *Earth-Sci. Rev.* **1980**, *16*, 319–355. [CrossRef]
80. Emmanuel, S.; Levenson, Y. Limestone weathering rates accelerated by micron-scale grain detachment. *Geology* **2014**, *42*, 751–754. [CrossRef]